Design of a Rapid Vacuum Pressure Swing Adsorption (RVPSA) Process for Post-combustion CO2 Capture from a Biomass-fuelled CHP Plant

Design of a Rapid Vacuum Pressure Swing Adsorption (RVPSA) Process for Post-combustion CO_2 Capture from a Biomass-fuelled CHP Plant

Mauro Luberti[a]*, Gabriel David Oreggioni[a,b], Hyungwoong Ahn[a]

[a]Scottish Carbon Capture and Storage Centre, Institute for Materials and Processes, School of Engineering, University of Edinburgh, Mayfield Road, Edinburgh, UK

[b]RCUK Centre for Sustainable Energy Use in Food Chains, Brunel University London, Uxbridge, Middlesex, UK

corresponding author: mauro.luberti@gmail.com

Abstract

It is aimed to design a novel RVPSA (Rapid Vacuum Pressure Swing Adsorption) unit for CO_2 concentration and recovery in order to achieve the aggressive CO_2 capture target, i.e. 95+% CO_2 purity and 90+% CO_2 recovery at the same time, applied to an existing 10 MW_{th} biomass-fuelled CHP plant. Biomass-fuelled CHP plants are principally carbon-neutral so there is no CO_2 addition to the atmosphere as a result of its operation if CO_2 emissions involved in soil enhancement, biomass transport and processing are ignored. Furthermore, integrating the biomass-fuelled CHP plant with carbon capture, transport and storage enables carbon-negative energy generation, as its net effect is to recover some CO_2 in the air and then store it underground through this plant operation. A RVPSA process features more efficient utilisation of the adsorbents in the column, leading to much higher bed productivity than a conventional adsorption process. Such a high bed productivity of a RVPSA makes it easier to scale up this process for its application to industrial post-combustion capture. A two-stage, two-bed RVPSA unit was designed and simulated to capture CO_2 from a biomass-fuelled CHP plant flue gas containing 13.3% CO_2 mole fraction. Effects of operating conditions such as the Purge-to-Feed ratio (P/F) and desorption pressure on the specific power consumption were investigated in detail. It was found that the productivity of the RVPSA unit designed in this study was 20-30 times higher than those of the conventional CO_2 capture VPSA processes.

***Keywords**: Biomass; CHP Plant; CO_2 Capture; Rapid Vacuum Pressure Swing Adsorption; Bed Productivity; Process Simulation*

1. Introduction

Our society still relies strongly on fossil fuels for production of heat and power it needs. A steady increase of the carbon dioxide concentration in the air has been observed, which is mainly due to an anthropogenic CO_2 that has been emitted into the air since industrial revolution. The increasing CO_2 content in the air, resulting in climate change and global warming, has spurred on R&D aiming to reduce anthropogenic carbon dioxide emissions. Various strategies to meet the future energy demand and reduce the CO_2 emission into the air simultaneously need to be developed, such as high efficiency energy production technologies, renewable energy technologies and carbon capture and storage (CCS) technologies.

Biomass has long been investigated both as a (nearly) CO_2 neutral substitute for fossil fuels and as a means for sequestering carbon in terrestrial ecosystems. More recently, the potential to integrate carbon capture and storage technologies with bio-energy systems has emerged as a promising way to capture atmospheric carbon through photosynthesis, producing energy from it and sequester it underground for geologic timescales (Obersteiner et al., 2001; Mollersten et al., 2003; Rhodes and Keith, 2008). In the marked contrast to CCS applied to fossil fuels, the BECCS (Bio-Energy Carbon Capture and Storage) is capable of reducing the CO_2 concentration in the air. In addition, the latest revisions of the IPCC report (IPCC, 2014) highlighted application of BECCS as a promising option for negative emission energy generation.

Up to now, relatively less attention has been paid to adsorption-based carbon capture research than conventional amine processes and other promising alternatives, such as solid- or chemical- looping and oxy-combustion (Mukherjee et al., 2015), when it is aimed to achieve 90+% CO_2 recovery and 95+% CO_2 purity for decarbonising fossil fuel-based power plants. However, both numerical simulation studies and lab- and pilot- scale experimental campaigns have been demonstrating that a well-designed CO_2 capture adsorption process can spend less energy (0.5-0.9 MJ_e/kg_{CO2}) (Krishnamurthy et al., 2014; Wang et al., 2013) than a conventional amine process (1.2-1.8 MJ_e/kg_{CO2}) (Ahn et al., 2013; IPCC, 2005) for post-combustion carbon capture. Compared to conventional systems, adsorption technology is, in fact, a more efficient option due to its easier operation, lower capital cost and lower energy consumption (Figueroa et al., 2008).

Recent literature reported simulation works mainly based on a two-stage VPSA process for post-combustion applications.

Kikkinides et al. (1993) were among the firsts to study the feasibility of recovering CO_2 from flue gas to generate a high-purity product by pressure swing adsorption. With activated carbon as the sorbent, CO_2 can be concentrated from 17% in the flue gas to almost pure CO_2 at the CO_2 recovery of 68.4%.

Park et al. (2002) studied a two-stage PSA process to recover 90% of the CO_2 contained in the flue gas containing 10-15% CO_2. Effects of the process configuration and operating variables were investigated.

Xiao et al. (2008) applied a VPSA process for CO_2 capture from a feed stream at 1.2 bar having 12% CO_2. A 12-step cycle including two equalizations and product purge was able to produce high purity CO_2 (> 95%) with a recovery greater than 70%. It was found that for zeolite 13X adsorbent the optimal feed temperature was around 67°C, to maximize the CO_2 working capacity.

Liu et al. (2011) simulated different cycles of VPSA processes using zeolite 5A for CO_2 capture from a gas mixture of 15% CO_2 and 85% N_2. At the feed pressure of 1.5 bar and the desorption pressure of 0.1 bar, it was not possible to achieve the CO_2 purity higher than 77% using a single-stage VPSA unit. To overcome the limit of the single-stage VPSA, they designed a two-stage VPSA consisting of a three-bed VPSA (first stage) and a two-bed VPSA (second stage). In the first stage, the CO_2 purity was increased to 70% and then this gas was recompressed to the second stage where the CO_2 purity increased up to 96%.

Shen et al. (2012) studied a two-stage VPSA process consisting of adsorption beds packed with activated carbon beads both theoretically and experimentally. They achieved the CO_2 purity of 95.3% and the CO_2 recovery of 74.4%.

Wang et al. (2012) studied a two-stage VPSA process using 13XAPG adsorbent and investigating the effects of operating conditions on the process performance. This process achieved the CO_2 purity of 96.5% and the CO_2 recovery of 93.4%.

Krishnamurthy et al. (2014) conducted pilot plant experiments of a VPSA process using 13X zeolite to separate CO_2 from N_2. The breakthrough experiments were first carried out confirming a near adiabatic behavior of the system. The CO_2 was concentrated to 95.9±1% with the recovery of 86.4±5.6%. To improve the process performance, a four-step cycle with light product pressurization using two beds was investigated. The optimized cycle was able to achieve 94.8±1% purity and 89.7±5.6% recovery.

Optimization on adsorptive CO_2-enriching processes were also performed to find optimal values of decision variables with several constraints (Ko et al., 2003; Delgado et al., 2011). The objectives of optimization were to achieve high CO_2 purity and recovery and minimize the power consumption.

Eventually, Webley (2014) carried out a perspective study on CO_2 capture adsorption technology, identifying major engineering obstacles to overcome as well as potential breakthroughs necessary to achieve its commercialization. He argued that a significant limitation for its scale-up lies in the vacuum pressure achievable by industrial vacuum pumps which is proportional to the gas flow rate, i.e. a vacuum pressure achievable at lab scale may not be reached at an industrial scale.

Moreover, there is still a concern with practicality of a commercial-scale CO_2 capture adsorption process lingering on due to it requiring humongous adsorption columns. But this issue can be overcome to some extent by advanced process design, given the fact that the size of the adsorption column can be drastically reduced by operating the adsorption process in a fast cyclic mode (e.g. RPSA process). In this work it was, therefore, sought to design a CO_2 capture RVPSA unit applied to an existing 10 MW_{th} biomass-fuelled CHP plant in order to achieve carbon-negative energy production. We will show that a CO_2 RVPSA unit can be designed to be affordable in size even at the industrial scale thanks to its intrinsic high productivity.

2. PSA mathematical model

A complete set of mathematical equations for predicting multi-component adsorption dynamics was constructed coupling mass, energy and momentum balances over a packed bed (Luberti et al., 2014).

Since the flow is assumed to be a dispersed plug flow the component mass balance is represented by:

$$-\frac{\partial}{\partial z}\left(D_z \cdot c_T \frac{\partial y_i}{\partial z}\right)+\frac{\partial c_i}{\partial t}+\frac{\partial (u \cdot c_i)}{\partial z}+\frac{1-\varepsilon}{\varepsilon}\cdot\frac{\partial \overline{q}_i}{\partial t}=0 \tag{1}$$

The overall mass balance for estimating the gas interstitial velocity along the column is:

$$\frac{\partial c_T}{\partial t}+\frac{\partial (u \cdot c_T)}{\partial z}+\frac{1-\varepsilon}{\varepsilon}\cdot\sum_{i=1}^{n}\frac{\partial \overline{q}_i}{\partial t}=0 \tag{2}$$

In this work the adsorption rate is represented by the Linear Driving Force (LDF) model:

$$\frac{\partial \overline{q}_i}{\partial t}=k_{LDF,i}\cdot(q_i^{*}-\overline{q}_i) \tag{3}$$

Since the column undergoes significant temperature excursions in both spatial and temporal domains caused by the heat of adsorption, the energy balance has to be taken into account as follows:

$$\begin{aligned}&(\hat{C}_{vg}\rho_g+\frac{1-\varepsilon}{\varepsilon}\cdot\hat{C}_{ps}\rho_s+\frac{1-\varepsilon}{\varepsilon}\cdot\hat{C}_{pg}\rho_{ads})\frac{\partial T}{\partial t}-\frac{RT}{\overline{M}}\frac{\partial \rho_g}{\partial t}-k_z\frac{\partial^2 T}{\partial z^2}\\&+\hat{C}_{pg}\rho_g u\cdot\frac{\partial T}{\partial z}-\frac{1-\varepsilon}{\varepsilon}\cdot\sum_{i=1}^{n}(-\Delta H_i)\frac{\partial \overline{q}_i}{\partial t}+\frac{4h_w}{D_c}\cdot(T-T_w)=0\end{aligned} \tag{4}$$

where the effect of the kinetic energy on adsorption dynamics was neglected (Luberti et al., 2015). Accordingly, the momentum balance is simplified into the Ergun equation by which the pressure drop along the column can be estimated as (Ergun, 1952):

$$-\frac{dP}{dz}=\frac{150\cdot\mu\cdot u\cdot(1-\varepsilon)^2}{d_P^2\cdot\varepsilon^2}+\frac{1.75\cdot(1-\varepsilon)\cdot\rho_g\cdot u\cdot|u|}{d_P\cdot\varepsilon} \quad (5)$$

In this study CO_2 is separated out of a binary mixture of CO_2 and N_2 using zeolite 13X pellets in the adsorption columns. The equilibrium isotherms of CO_2 and N_2 adsorption on zeolite 13X are estimated by the following extended mono-site binary-component Langmuir isotherms:

$$q_i^*=\frac{q_{si}\cdot b_i\cdot P_i}{1+\sum_{i=1}^{n} b_i\cdot P_i} \quad (6)$$

where $b_i=b_{i0}\cdot\exp(-\Delta H_i/RT)$

The Langmuir isotherm constants were obtained by regression of the experimental data in the range of the operating pressure and temperature (Xiao et al., 2008) using Origin 8.5 software (OriginLab, 2010). The heat of adsorption generally varies with adsorbed amount due to the heterogeneity of adsorption sites (Myers, 2002); however it is kept constant regardless of adsorbed amount since the extended mono-site Langmuir isotherm was chosen in this study (Ruthven, 1984).

The axial mass dispersion coefficient D_z and the axial thermal dispersion coefficient k_z are estimated using the following correlations proposed by Wakao and Funazkri (1978):

$$\frac{\varepsilon\cdot D_z}{D_m}=20+0.5\cdot Sc\cdot \mathrm{Re} \quad (7)$$

$$\frac{k_z}{k_g}=7+0.5\cdot \mathrm{Pr}\cdot \mathrm{Re} \quad (8)$$

General properties of the gases, like thermal conductivity, viscosity, and molar specific heat as well as diffusivity coefficients were obtained according to Bird et al. (2007). The industrial columns were supposed to be adiabatic which is in agreement with what reported by Krishnamurthy et al. (2014).

The boundary conditions for all the steps constituting a conventional Skarstrom cycle are presented in Table 1.

Table 1: Boundary conditions associated with the steps in RVPSA simulation

Adsorption	
z = 0	**z = L**
$-D_z c_T\frac{\partial y_i}{\partial z}=u\cdot(c_{f,i}-c_i)$	$\frac{\partial y_i}{\partial z}=0$
$u=u_f$	$P=P_{ads}$

$-k_z \frac{\partial T}{\partial z} = u \cdot \rho_g \cdot \hat{C}_{pg} \cdot (T_f - T)$	$\frac{\partial T}{\partial z} = 0$
Blowdown	
z = 0	**z = L**
$\frac{\partial y_i}{\partial z} = 0$	$\frac{\partial y_i}{\partial z} = 0$
$\frac{\partial P}{\partial t} = \alpha \cdot (P_{des} - P)$	$u = 0$
$\frac{\partial T}{\partial z} = 0$	$\frac{\partial T}{\partial z} = 0$
Product purge	
z = 0	**z = L**
$\frac{\partial y_i}{\partial z} = 0$	$-D_z c_T \frac{\partial y_i}{\partial z} = u \cdot (c_{p,i} - c_i)$
$P = P_{des}$	$u = u_p$
$\frac{\partial T}{\partial z} = 0$	$-k_z \frac{\partial T}{\partial z} = u \cdot \rho_g \cdot \hat{C}_{pg} \cdot (T_p - T)$
Feed pressurisation	
z = 0	**z = L**
$-D_z c_T \frac{\partial y_i}{\partial z} = u \cdot (c_{f,i} - c_i)$	$\frac{\partial y_i}{\partial z} = 0$
$\frac{\partial P}{\partial t} = \alpha \cdot (P_{ads} - P)$	$u = 0$
$-k_z \frac{\partial T}{\partial z} = u \cdot \rho_g \cdot \hat{C}_{pg} \cdot (T_f - T)$	$\frac{\partial T}{\partial z} = 0$

During the pressurisation and blowdown steps, the change of bed pressure at the feed end with time is determined by a linear differential equation expressed by:

$$\frac{dP}{dt} = \alpha \cdot (P_f - P) \tag{9}$$

where P_f is either the adsorption or purge pressures determined by operating conditions and α (s^{-1}) represents a rate constant determining how quickly the pressure change occurs, indicating that controlling α is equivalent to changing the opening of a metering valve on the gas stream connecting the column to the surroundings.

In a CO_2 enrichment process by a CO_2 capture VPSA where carbon dioxide is the most strongly adsorbed component, the CO_2 product is extracted during blowdown and purge steps. The cycle performance parameters are defined in this case as follows:

$$CO_2\ Purity = \frac{\int_0^{t_{BD}} C_{CO_2} u\big|_{z=0}\, dt + \int_0^{t_{PU}} C_{CO_2} u\big|_{z=0}\, dt}{\sum_i^n \int_0^{t_{BD}} C_i u\big|_{z=0}\, dt + \sum_i^n \int_0^{t_{PU}} C_i u\big|_{z=0}\, dt} \tag{10}$$

$$CO_2\ \mathrm{Recovery} = \frac{\int_0^{t_{BD}} C_{CO_2} u\big|_{z=0}\, dt + \int_0^{t_{PU}} C_{CO_2} u\big|_{z=0}\, dt}{\int_0^{t_{AD}+t_{PR}} C_{CO_2} u\big|_{z=0}\, dt} \tag{11}$$

$$CO_2\ \mathrm{Productivity} = \frac{\left(\int_0^{t_{BD}} C_{CO_2} u\big|_{z=0}\, dt + \int_0^{t_{PU}} C_{CO_2} u\big|_{z=0}\, dt\right)\cdot A_c}{t_{cycle}\cdot M_{ads}} \tag{12}$$

$$Specific\ \ power = \frac{\int_0^{t_{AD}+t_{PR}} power_{blower}\, dt + \int_0^{t_{BD}+t_{PU}} power_{vacuum}\, dt}{\left(\int_0^{t_{BD}} C_{CO_2} u\big|_{z=0}\, dt + \int_0^{t_{PU}} C_{CO_2} u\big|_{z=0}\, dt\right)\cdot A_c} \tag{13}$$

$$power_{blower} = F\cdot\overline{M}\cdot\frac{\gamma}{\gamma-1}\cdot\left(\frac{110kPa}{\rho_g}\right)\cdot\left[\left(\frac{P_{ads}}{110kPa}\right)^{\frac{\gamma-1}{\gamma}} - 1\right] \tag{14}$$

$$power_{vacuum} = F\cdot\overline{M}\cdot\frac{\gamma}{\gamma-1}\cdot\left(\frac{P_{des}}{\rho_g}\right)\cdot\left[\left(\frac{110kPa}{P_{des}}\right)^{\frac{\gamma-1}{\gamma}} - 1\right] \tag{15}$$

where the Eqs. (13) to (15) relate to calculation of the specific power required to achieve the separation. This power consumption is calculated directly by dividing the sum of the power consumption in running the blower and vacuum pump by the amount of CO_2 captured after cyclic steady state (CSS) is achieved.

In all the simulations the set of equations were solved numerically by gPROMS software (PSE, 2010). The spatial domain along the column was discretized by the second order orthogonal collocation on finite elements method (OCFEM) with 100 nodes where the absolute and relative numerical accuracies were both set to 10^{-5} (Ahn et al., 2014).

3. Simulation results

3.1 Biomass gasification CHP plant

This study is based on a biomass gasification CHP plant running with a gas engine that is in operation in Gussing, Austria (Simader, 2004). In the process, the biomass feed is converted into a syngas with a Fast Internally Circulating Fluidized Bed (FICFB) process and then the syngas is fed to a gas engine (GE Jenbacher Type 6) for power generation. In addition to power, heat can also be generated by recovering heat from both gasifier and gas engine. The biomass CHP plant was designed and simulated on the basis of around 10 MW_{th}

thermal input of biomass feed. All the details of this process as well as a comprehensive simulation methodology can be found elsewhere (Oreggioni et al., 2015). The process flowsheet is shown in Figure 1.

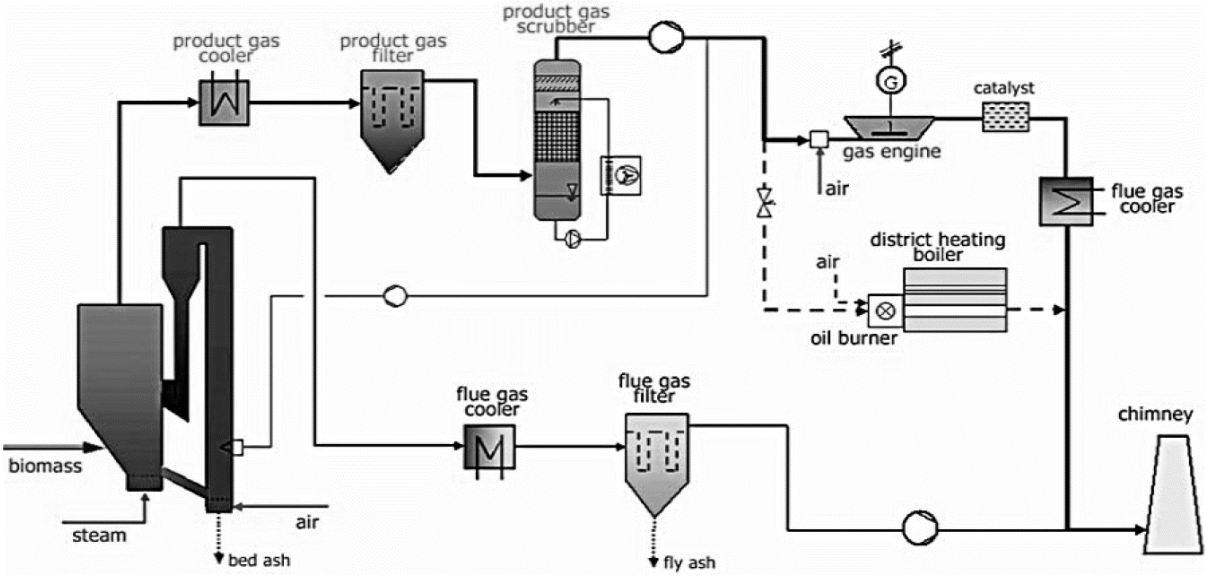

Figure 1: Process flowsheet of the 10 MW_{th} biomass-fuelled CHP plant (Simader, 2004)

A RVPSA unit has been designed to capture 90% CO_2 from the flue gas prior to discharging it to atmosphere. The pressure, temperature, composition and flowrate of the flue gas stream were estimated by the plant data (Simader, 2004) and the simulation results (Oreggioni et al., 2015) as summarised in Table 2. For simplicity it was assumed that the oxygen existing in the flue gas would behave similarly to nitrogen, so that the oxygen was replaced by nitrogen in the flue gas: this assumption has been commonly adopted in the literature (Krishnamurthy et al., 2014; Liu et al., 2011; Wang et al., 2012). Zeolite 13X was chosen as adsorbent for the RVPSA in this work. Several researchers (Krishnamurthy et al., 2014; Xiao et al., 2008; Wang et al., 2012) have also designed successfully conventional, not rapid VPSA cycles using zeolite 13X for carbon capture from the flue gases of PC-fired boiler power plants. The physical properties of the zeolite 13X pellet and the associated equilibrium isotherm parameters as well as the column parameters are listed in Table 3.

Table 2: CHP plant flue gas stream information (dry basis)

Parameter (unit)	Value
Total flowrate (kmol/h)	789.0
Pressure (kPa)	110.0
Temperature (K)	298.15
CO_2 mole fraction (mol%)	13.3 (balanced with N_2)

Table 3: List of adsorbent and column parameters used for the RVPSA simulations

Column parameters	
External bed void fraction, ε (-)	0.37
Axial mass dispersion coefficient, D_z (m^2/s)	$5.9x10^{-3}$
Axial thermal dispersion coefficient, k_z (W/m·K)	3.8
Wall heat transfer coefficient, h_w ($W/m^2·K$)	0.0
13X Zeolite parameters	
Adsorbent density, ρ_s (kg/m^3)	1,017
Specific heat capacity (J/kg·K)	920
Particle diameter (mm)	2.5
$k_{LDF,CO2}$ / $k_{LDF,N2}$ (s^{-1})	19.3 / 19.4
$q_{s,CO2}$ / $q_{s,N2}$ (mol/kg)	3.9 / 3.9
$b_{0,CO2}$ / $b_{0,N2}$ (bar^{-1})	$3.1x10^{-5}$ / $1.0x10^{-4}$
$-\Delta H_{CO2}$ / $-\Delta H_{N2}$ (J/mol)	32,186 / 14,875

3.2 RVPSA unit design

A two-stage RVPSA unit each of which consists of two adsorption columns was designed to capture CO_2 from the flue gas of the 10 MW_{th} biomass-fuelled CHP plant. It has been reported that such a two-stage RVPSA unit could achieve CO_2 recovery as high as 90% and CO_2 purity higher than 95% (Wang et al., 2012; Shen et al., 2012) when applied to a flue gas stream containing 10 – 16% CO_2 on the molar basis as post-combustion carbon capture. Moreover, since the total feed flowrate is very high, two RVPSA units in parallel were designed for the first stage in order to reduce the pressure drops. The resulting volumetric flowrate flowing into a single RVPSA unit was 1.81 m^3/s. Figure 2 shows the diagram of the two-stage, two-bed RVPSA unit: note that the second RVPSA unit has a smaller size compared to the units of the first stage. A buffer tank is installed between the two stages to mix and store the CO_2 product from the first stage (Figure 2).

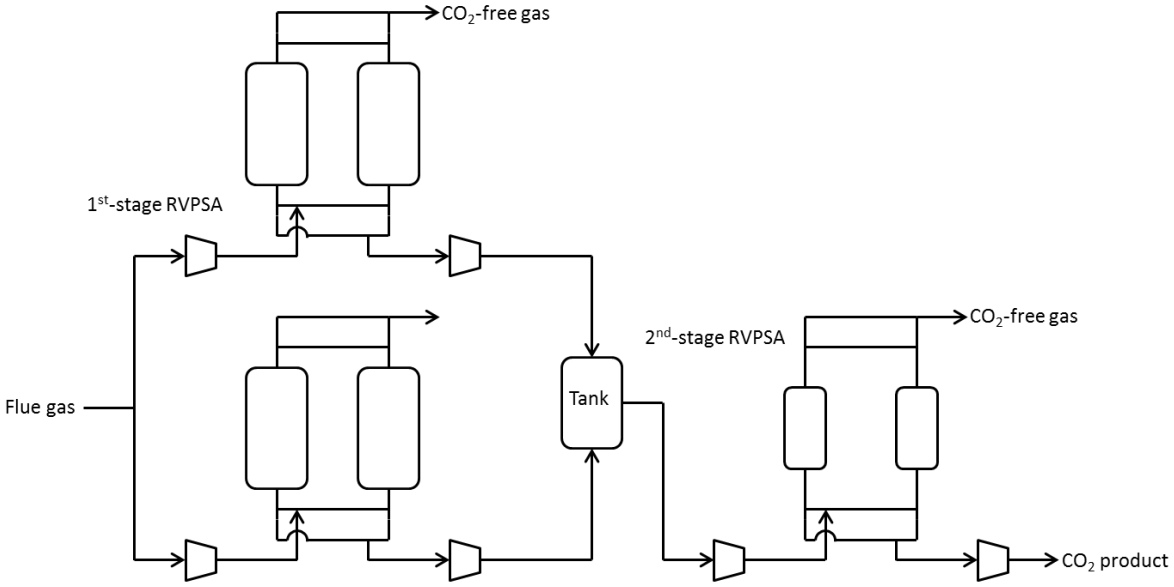

Figure 2: Schematic diagram of the two-bed two-stage RVPSA unit

The cycle of each two-bed RVPSA stage was configured with four-step Skarstrom cycle as shown in Figure 3. The performances of the RVPSA units were evaluated with the parameters presented in the previous section of this study. In particular, because of the mechanical losses, the actual power consumptions of the vacuum pump and blower are likely to be greater than those estimated by Eqs. (14) and (15). Therefore, the predicted power consumptions by Eqs. (14) and (15) will be used for the comparison of the process performances reported in the literature (Park et al., 2002; Wang et al., 2012).

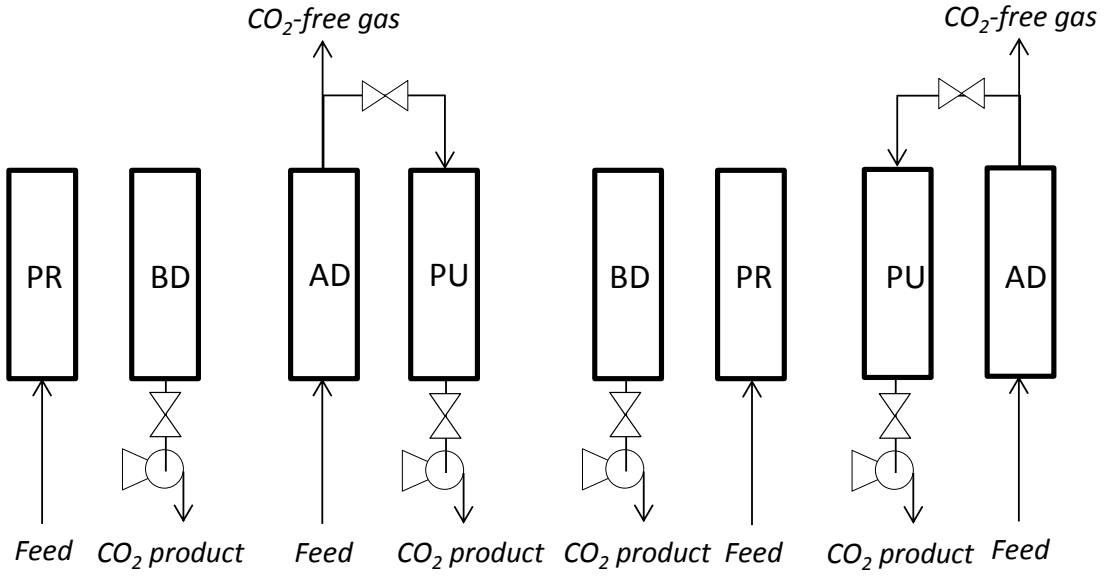

Figure 3: Two-bed four-step Skarstrom configuration with AD: adsorption; BD: countercurrent blowdown; PU: countercurrent product purge; PR: feed pressurisation

(t_{cycle} = 18 s; t_{AD} = t_{PU} = 8 s; t_{BD} = t_{PR} = 1 s)

The 1st stage RVPSA is deemed as a CO_2 enriching stage where the CO_2 mole fraction is increased from 13.3% up to 55.0% with the CO_2 recovery sufficiently higher than 90%. The following 2nd stage RVPSA is regarded as a CO_2 purification step for increasing the CO_2 mole fraction up to 95% at the sacrifice of the CO_2 recovery in order to achieve the overall 90% CO_2 capture rate. Table 4 shows the column dimensions and the operating conditions of the two-stage VPSA units investigated in this work.

Table 4: Column dimensions and operating conditions for the two-stage RVPSA units

	P_{feed} (kPa)	T_{feed} (K)	t_{cycle} (s)	Q_{unit} (m^3/s)	D_c (m)	L_c (m)	u (m/s)	ΔP (kPa)
1st-stage RVPSA	166	298.15	18	1.81	1.2	1.2	1.60	16
2nd-stage RVPSA	156	298.15	18	0.86	1.0	1.0	1.09	6

For the RVPSA process the total cycle time was fixed as 18 s for both the stages with t_{AD} = t_{PU} = 8 s and t_{BD} = t_{PR} = 1 s. The value of α was set at 10 s^{-1} to avoid excessive velocities during the pressure-varying steps. Since the feed flowrate is to be determined by the upstream operations and the adsorption pressure is to be fixed at the typical value of 150 kPa (Khrisnamurty et al., 2014; Wang et al., 2012), each column has to be sized so as to obtain a reasonable pressure drop along the column. Therefore, the column diameter was fixed at 1.2 m for the first stage and as 1.0 m for the second stage. With the same L/D = 1 the resulting pressure drops were evaluated at 16 kPa and 6 kPa, respectively for the first and second stage. For the second stage we considered the best simulation obtained from the first stage, as it will be discussed in the next sub-section.

Unlike industrial conventional PSA fixed beds where superficial velocities usually range between 0.1 and 0.5 m/s, in the RVPSA units of this study the superficial velocity was as high as 1.6 m/s for the first stage and 1.1 m/s for the second stage. Higher velocities are beneficial to achieve enhanced bed productivities which are typical of RPSA cycles, but they have the negative effect of having higher pressure drops, and hence higher power consumptions of blowers. Irrespective of the pressure drop, it is required to compress the feed gas up to 150 kPa from 110 kPa in order to create the sufficient working capacity of adsorbents between adsorption and desorption conditions. If pressure drops become large there is a need to compress the feed to a pressure higher than 150 kPa to overcome the pressure drop and maintain the working capacity at the same time. Figure 4 shows the pressure drops along the columns for the two stages of RVPSA units. For direct comparison

of the two stages the pressure profiles have been plotted against a common dimensionless axial coordinate, defined as position in the column over total length (z/L).

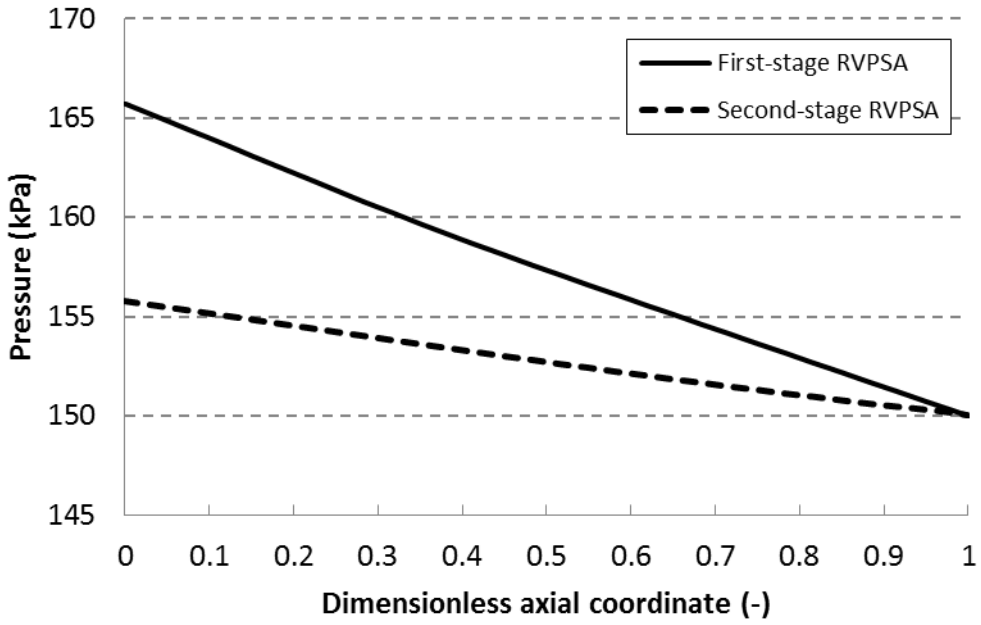

Figure 4: Pressure drops along the columns for the two stages of RVPSA units at the end of the adsorption step: the X-axis reports a common dimensionless axial coordinate

3.3 Effects of P/F ratio and desorption pressure on RVPSA performances

In general it is expected that the CO_2 recovery will be improved with decreasing desorption pressure, decreasing superficial velocity, shorter adsorption time and higher P/F ratio, all of which can prevent CO_2 in the feed from penetrating into the top end of the column during the adsorption step. This is because the CO_2 recovery is inversely proportional to the amount of CO_2 loss during the adsorption step. Conversely the CO_2 purity will be reduced with the abovementioned changes of operating conditions except for the desorption pressure. In this work, P/F denotes the ratio of the molar purge flowrate of one column during the purge step to the molar feed flowrate of one column during the adsorption step. By and large the power consumption of the RVPSA unit highly depends on the choice of desorption pressure if the P/F ratio is low enough especially for achieving a very high CO_2 product purity or it changes within a narrow range. To avoid excessive power consumption, therefore, it would be preferable to operate a RVPSA unit at as high a desorption pressure as possible. However, running a RVPSA at a high desorption pressure should be compensated by increasing P/F ratio, decreasing adsorption time, or decreasing superficial velocity in order to maintain the CO_2 recovery as high as possible.

In the following parametric study, it was sought to find the optimal operation conditions at which the RVPSA could minimise the power consumption, meeting the CO_2

purity and recovery requirements. To this end, the effects of P/F ratio and desorption pressure were investigated in terms of process performances such as CO_2 purity, CO_2 recovery, bed productivity and specific power consumption summing the compression power during pressurisation and adsorption steps and the evacuation power during blowdown and purge steps. Figure 5 shows the effect of the P/F ratio on CO_2 purity, CO_2 recovery and bed productivity in the first stage RVPSA running at the fixed desorption pressure of 10 kPa. As expected, with increasing P/F ratio the CO_2 recovery increased while the purity decreased. The bed productivity also increased similarly to the CO_2 recovery, as the cycle time was kept constant. The specific power consumptions shown in Figure 6 were calculated on the basis of the CO_2 product obtained during the blowdown and purge steps. It can be seen that the specific power consumption of the compressor decreases with the increase of the P/F ratio, in spite of the total compression power consumption not varying. This is due to the amount of CO_2 product increasing with the P/F ratio. Contrary to the compressor, the specific power consumption of the vacuum pump increased with the P/F ratio as the gas flowrate through the vacuum pump must have increased with the increasing P/F ratio. Given that the vacuum pump spent greater power than the compressor, the overall specific power consumption increased monotonically with the P/F ratio. Similar trends were also observed in the literature (Park et al., 2002).

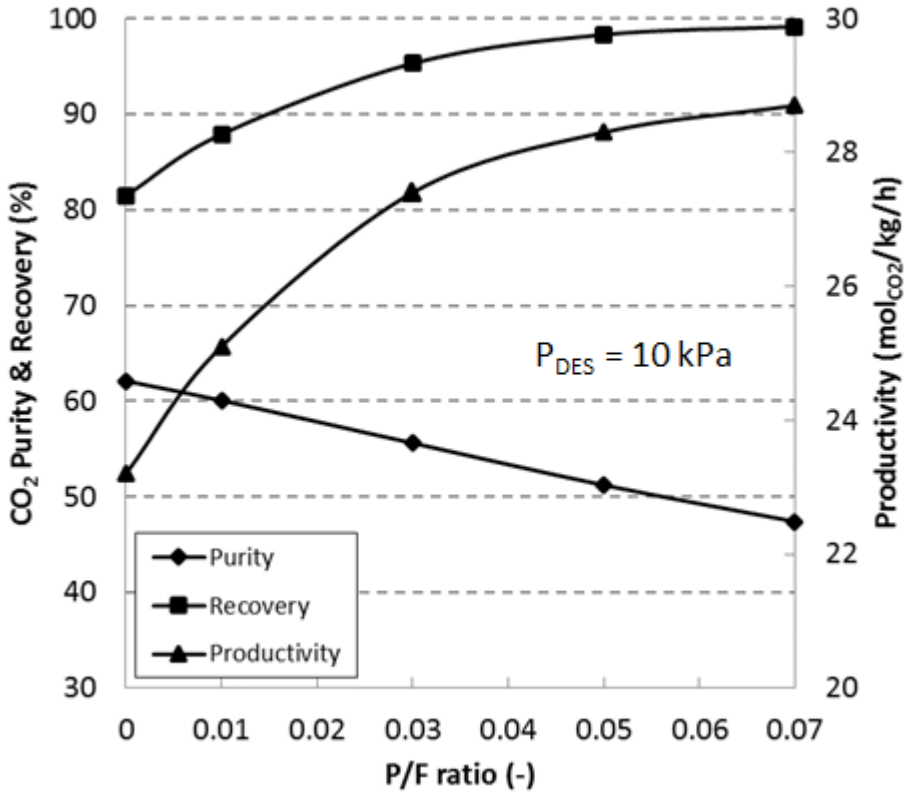

Figure 5: Evolution of CO_2 purity, CO_2 recovery and bed productivity with the P/F ratio for the first stage RVPSA at a desorption pressure of 10 kPa

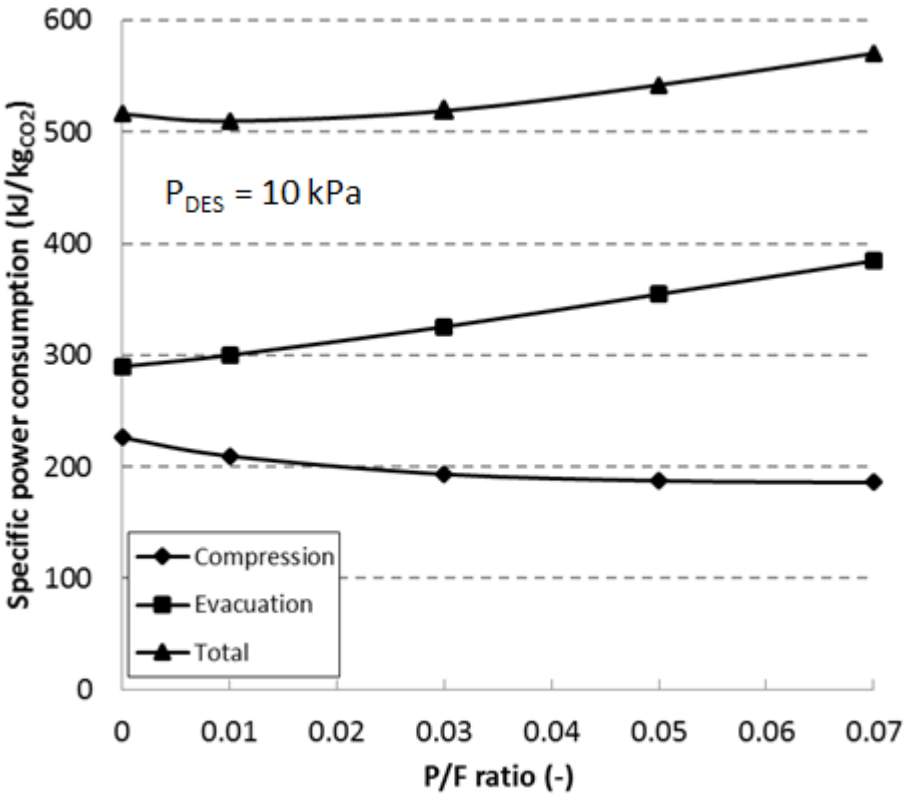

Figure 6: Evolution of specific power consumption with the P/F ratio for the first stage RVPSA at a desorption pressure of 10 kPa

It was also investigated the effect of the desorption pressure on the CO_2 purity, CO_2 recovery and bed productivity for the first stage RVPSA with the P/F ratio fixed at 0.03, as shown in Figure 7. In this case with an increase of desorption pressure the CO_2 recovery and bed productivity decreased due to the reduced working capacity of the adsorbents. By contrast, the CO_2 purity was not affected much by the changing desorption pressure due to the constant selectivity of CO_2 over N_2 of the zeolite 13X imposed by the Langmuir isotherm. As shown in Figure 8, operating the RVPSA at a higher desorption pressure could reduce the specific power consumption of the vacuum pump. On the other hand, the specific compression power consumption increased because of the CO_2 recovery decreasing with the desorption pressure. The optimal simulation selected for the following second stage study was the one having P/F = 0.03 and P_{DES} = 7.5 kPa. Since with P/F = 0.03 the CO_2 purity was high enough and did not change much (54-56%) in the entire range of desorption pressure, it was aimed to maximize the desorption pressure still maintaining the CO_2 recovery much higher than 90%. The resulting performances were the following: CO_2 purity of 55.0%, CO_2 recovery of 98.3%, bed productivity of 28.1 mol_{CO2}/kg/h and total power consumption of 569.7 kJ/kg_{CO2}.

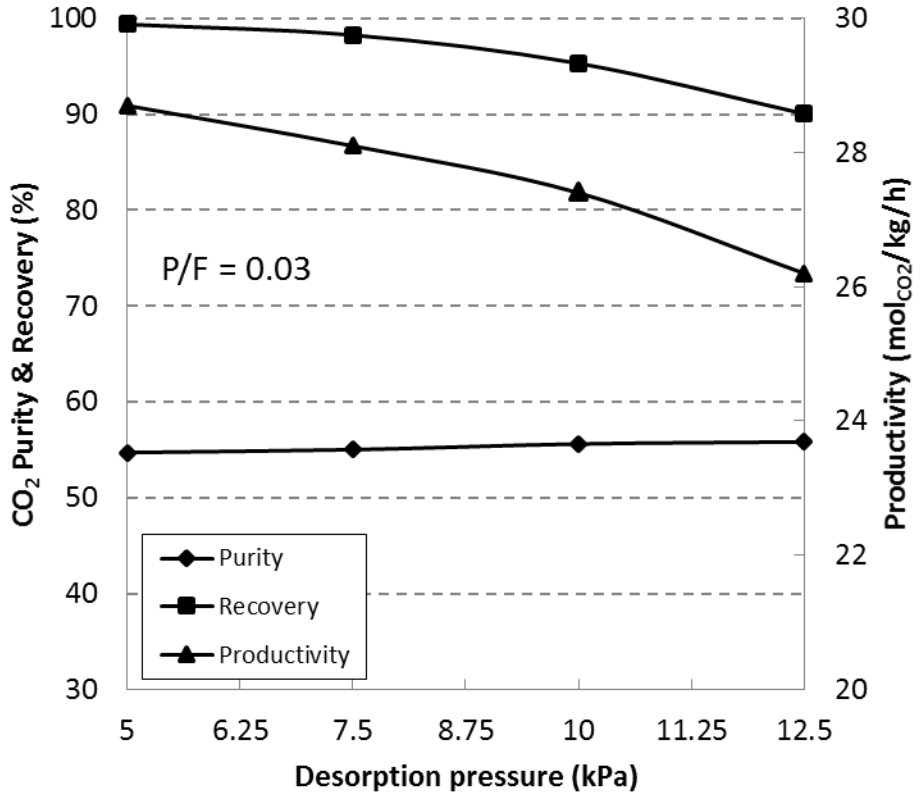

Figure 7: Evolution of CO_2 purity, CO_2 recovery and bed productivity with the desorption pressure for the first stage RVPSA at a P/F ratio of 0.03

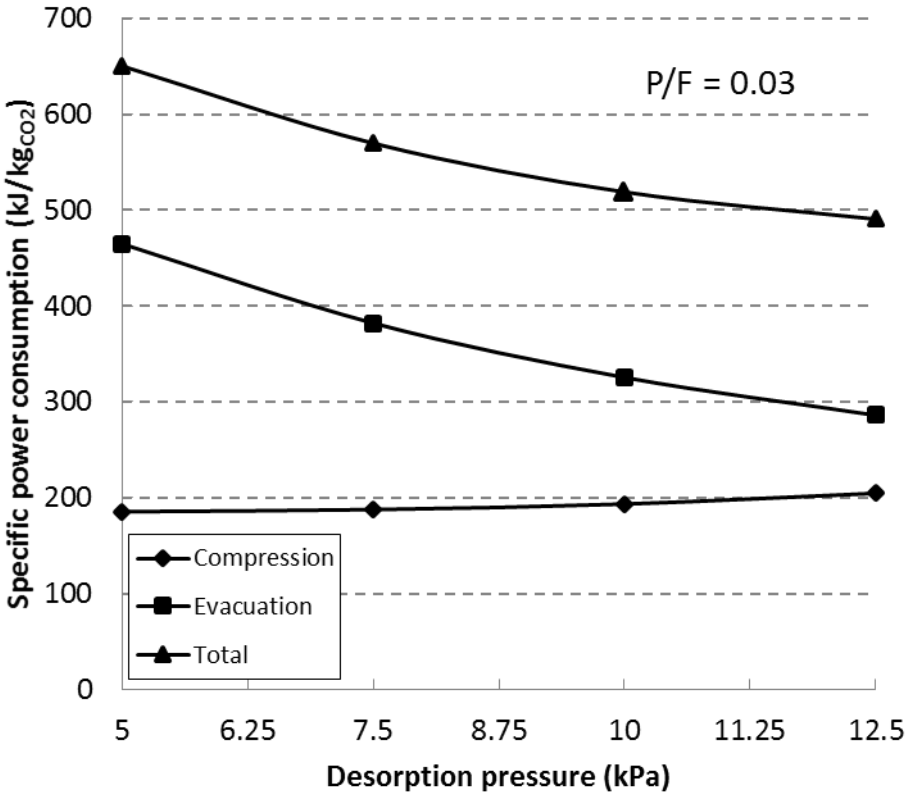

Figure 8: Evolution of specific power consumption with the desorption pressure for the first stage RVPSA at a P/F ratio of 0.03

Similarly to the first stage, Figures 9 and 10 exhibit the effect of the P/F ratio on the second stage RVPSA performances with the desorption pressure fixed at 7.5 kPa. It should be noted that since the CO_2 purity and recovery changed little in the range of selected P/F ratios (Figure 9), the specific power consumptions were almost constant (Figure 10). At P/F = 0.01 the CO_2 purity could rise up to 95% while the recovery was still sufficiently higher than 90%, meeting the overall 90% CO_2 capture target. The bed productivity of the second stage was much higher (94.3 mol_{CO2}/kg/h) than the first one, due to its CO_2 recovery being very high and less amount of the adsorbents being required for the second stage.

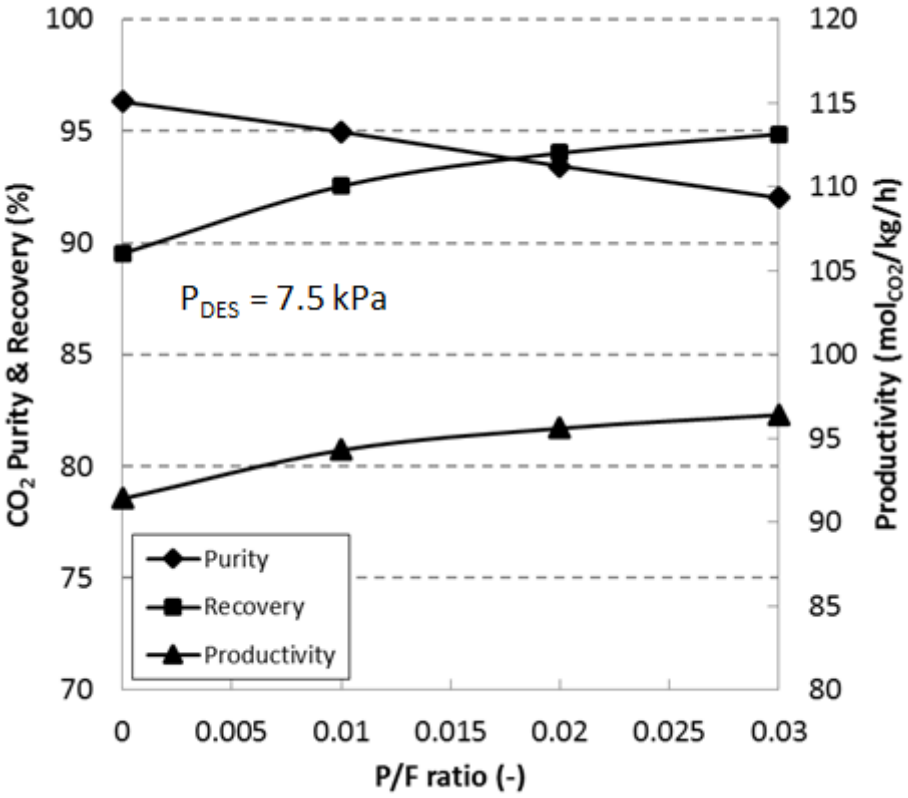

Figure 9: Evolution of CO_2 purity, CO_2 recovery and bed productivity with the P/F ratio for the second stage RVPSA at a desorption pressure of 7.5 kPa

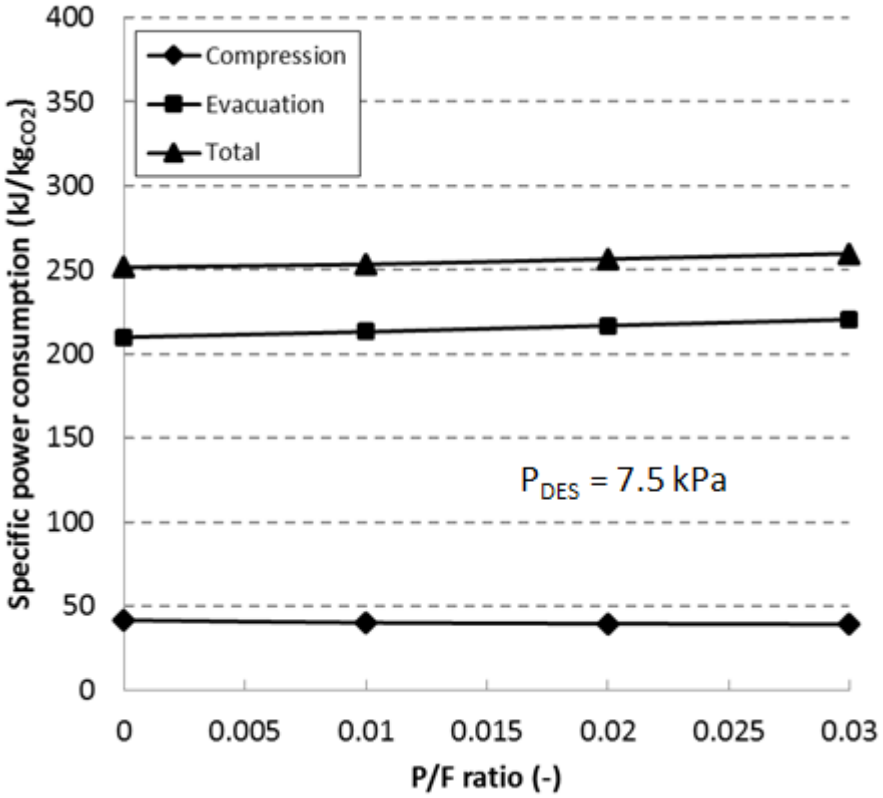

Figure 10: Evolution of specific power consumption with the P/F ratio for the second stage RVPSA at a desorption pressure of 7.5 kPa

Figure 11 shows the CO_2 mole fraction profiles along the column at the end of adsorption step of both the first and second stage RVPSA simulations at its CSS (Cyclic Steady State). This comparison could explain clearly why the CO_2 recovery at the first stage could be maintained high (i.e. insignificant loss of CO_2 during adsorption) whilst the CO_2 purity at the second stage was improved greatly (i.e. the column highly saturated with CO_2 during adsorption).

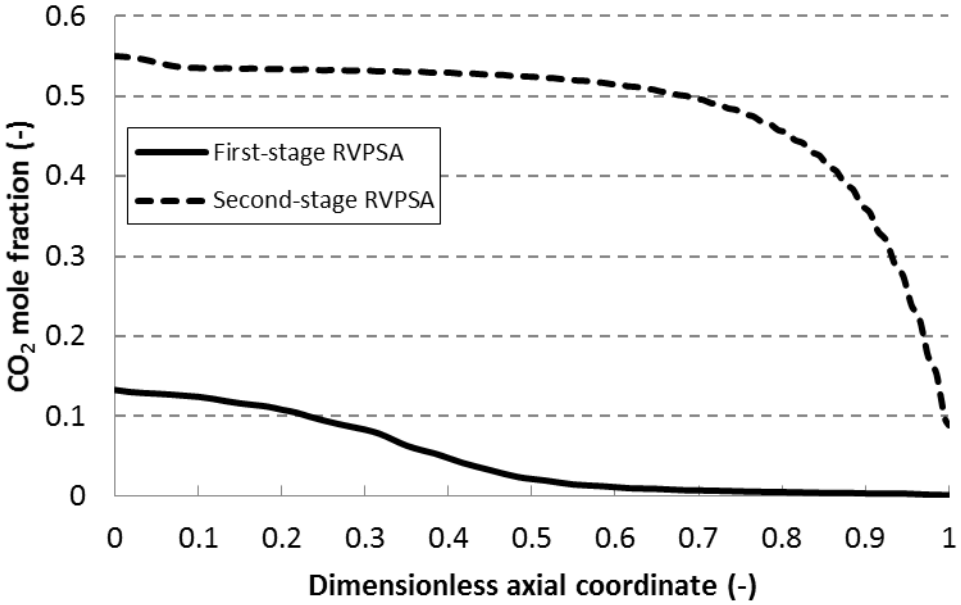

Figure 11: CO_2 mole fraction along the columns for the two stages of RVPSA units at the end of the adsorption step at its CSS: the X-axis reports a common dimensionless axial coordinate (First-stage: P/F = 0.03, P_{des} = 7.5 kPa; Second-stage: P/F = 0.01, P_{des} = 7.5 kPa)

3.4 Integrated two-stage RVPSA simulation results

Connecting the two RVPSA processes in series, the estimated overall performance was: CO_2 recovery = 90.9%, CO_2 purity = 95.0%, bed productivity = 21.2 mol_{CO2}/kg/h, specific power consumption = 822.9 kJ/kg_{CO2}. Table 5 summarises the performances of each RVPSA stage and the overall process after its CSS was reached. As shown in the table, the first stage accounted for around 69% of the total energy consumption and the vacuum pump of the first stage took a share of about 46% of the total energy consumption. These results were similar to those reported by other studies (Liu et al., 2011; Wang et al., 2013). The overall mass balance of the integrated two-stage process is shown in Figure 12.

Table 5: Summary of the two-stage RVPSA process performances

	CO_2 Purity (%)	CO_2 Recovery (%)	Bed Productivity (mol_{CO2}/kg/h)	Specific power consumption (kJ/kg_{CO2})		
				Compression	Evacuation	Total
1^{st}-stage RVPSA	55.0	98.3	28.1	187.6	382.1	569.7
2^{nd}-stage RVPSA	95.0	92.5	94.3	40.1	213.1	253.2
Two-stage RVPSA	95.0	90.9	21.2	227.7	595.2	822.9

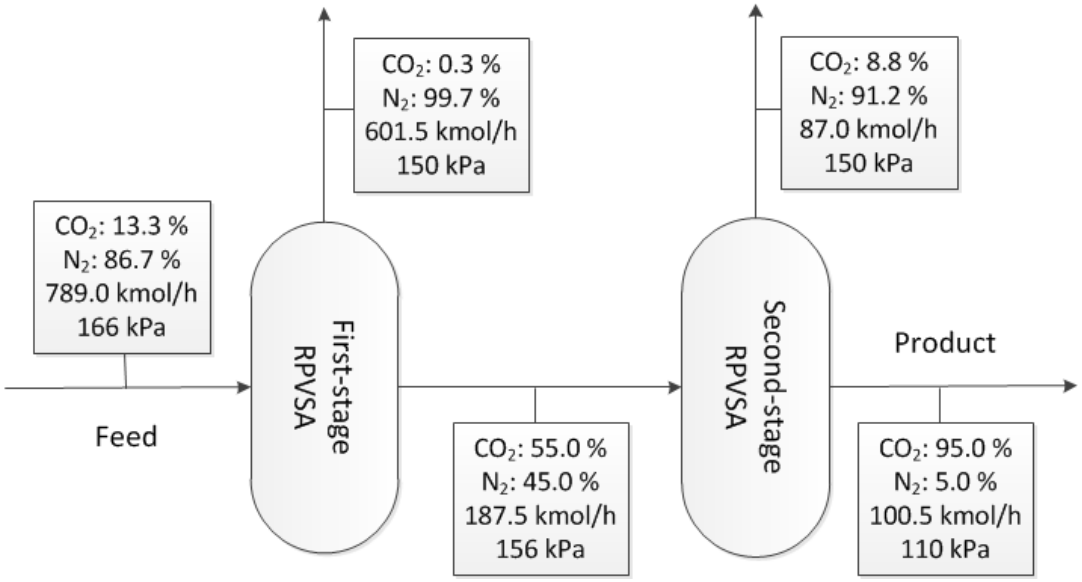

Figure 12: Overall mass balance of the two-stage RVPSA process for capturing CO_2 from the flue gas of the 10 MW_{th} biomass CHP plant

Eventually, Table 6 shows comparison of our two-stage rapid VPSA unit with other adsorptive processes designed for post-combustion CO_2 capture. All the results were based on simulations using an adiabatic efficiency equal to 100% for the turbomachineries. As it can be seen from Table 6, in all the two-stage VPSA processes the CO_2 content in the feed is in the range of 10-16 mol% while the desorption conditions vary from 5 to 20 kPa. Compared with the other works the CO_2 purity and CO_2 recovery of this study are in the usual range of the targeted conditions. Only the simulations carried out by Shen et al. (2012) showed a slightly lower CO_2 recovery due to the use of activated carbon as adsorbent. Even if activated carbons have relative low CO_2 capacity and low selectivity of CO_2/N_2 in comparison with zeolites, the authors have selected these adsorbents because they are water tolerant, they can be produced with novel morphologies and they are less expensive than zeolites. Krishnamurthy et al. (2014) reported very low energy consumption for their single stage VPSA unit but it should be noted that the desorption conditions were extremely low (1-2 kPa). In terms of power consumption this work resulted in the upper part of the range: this could be explained partly by its rapid cycle operation featuring a high interstitial gas velocity during adsorption leading to a broader CO_2 concentration front.

However, the specific power consumption of this study could be reduced by advancing the step configuration of a cycle. It is likely that addition of a pressure equalisation step or a heavy reflux step into a cycle would improve the CO_2 purity greatly. Such an advanced cycle will allow the adsorption system to meet the CO_2 purity requirement even at a higher desorption pressure or a lower P/F ratio, resulting in lower power consumption.

It should be noted that at the sacrifice of the increased power consumption the two-stage rapid VPSA cycle could achieve an excellent bed productivity that would be essential

to scale up the CO_2 capture adsorptive process for its industrial application. The bed productivity of our RVPSA unit was 20-30 times higher than those of the other works. Such a high bed productivity was achievable only by running the VPSA units with a very short cycle time of only 18 seconds.

Table 6: Comparison of performances of several simulated CO_2 capture processes using VPSA technology

Process	Adsorbent	$y_{CO2,feed}$ (%)	No. beds	Desorption condition	P/F ratio (-)	Purity (%)	Recovery (%)	Power consumption (kJ/kg_{CO2})	Productivity (mol_{CO2}/ kg/h)	Reference
2-stage RVPSA	13X	13.3	2	7.5 kPa	1^{st}: 0.03 2^{nd}: 0.01	95.0	90.9	822.9	21.2	This study
2-stage VPSA	$13X_{APG}$	15.0	1^{st}: 3 2^{nd}: 2	10 kPa	1^{st}: 0.25 2^{nd}: 0.05	96.5	93.4	528.4	0.71	Wang et al., 2012
2-stage VPSA	$13X_{APG}$	15.0	1^{st}: 3 2^{nd}: 2	6 kPa	1^{st}: 0.25 2^{nd}: 0.05	96.6	97.9	594.0	0.72	Wang et al., 2012
2-stage VPSA	AC beads	15.0	2	10 kPa	1^{st}: N/A[1] 2^{nd}: X[2]	95.3	74.4	723.6	0.85	Shen et al., 2012
2-stage VPSA	AC beads	15.0	2	5 kPa	1^{st}: N/A[1] 2^{nd}: X[2]	96.3	80.7	829.3	0.93	Shen et al., 2012
2-stage VPSA	1^{st}:$13X_{APG}$ 2^{nd}:ACBs	16.0	1^{st}: 3 2^{nd}: 2	1^{st}: 7.5 kPa 2^{nd}: 20 kPa	1^{st}: 0.09 2^{nd}: X[2]	95.2	91.3	756.0	0.81	Wang et al., 2013
2-stage VPSA	13X	10.5	2	1^{st}: 6.7 kPa 2^{nd}: 13.3 kPa	1^{st}: 0.06 2^{nd}: X[2]	99.0	80.0	513.2	//	Cho et al., 2004
2-stage VPSA	5A	15.0	1^{st}: 3 2^{nd}: 2	10 kPa	1^{st}: 0.25 2^{nd}: 0.18	96.1	91.1	645.7	0.33	Liu et al., 2011
1-stage VPSA	13X	15.0	2	1.1 kPa	X[2]	97.9	80.6	524.4	0.84	Krishnamurthy et al., 2014
1-stage VPSA	13X	15.0	2	2.2 kPa	X[2]	97.0	93.3	498.1	0.77	Krishnamurthy et al., 2014

1: N/A means P/F value not available; 2: X means purge step not present in the cycle

4. Conclusions

A cyclic adsorption process has been proposed by many researchers as a promising CO_2 capture process that requires less energy than conventional amine process. It has been proven both experimentally and numerically that an adsorptive capture process could capture CO_2 more economically than the conventional amine process, meeting the CO_2 purity and recovery targets. However, there is still uncertainty on how easily an adsorptive capture unit can be scaled up for its industrial application, as most of the past studies were carried out at a lab scale.

In this study, we proposed a solution to this scale-up issue. The bed productivity must be improved significantly to reduce the size of adsorption column and it is achievable by operating the adsorption cycle rapidly. A two-stage, two-bed RVPSA unit was designed and simulated to capture CO_2 from the flue gas of an existing 10 MW_{th} biomass-fuelled CHP power plant. This kind of plants are emerging as a promising technological option for negative emission energy generation. In this work the integrated RVPSA unit included a first stage where CO_2 purity was increased from 13.3% to 55%; this gas was then recompressed and sent to a second stage where CO_2 purity increased up to 95%. The overall CO_2 recovery of this process was 90.9% with an energy consumption of 822.9 kJ/kg_{CO2}. Moreover, the bed productivity of the overall RVPSA unit was 21.2 $mol_{CO2}/kg/h$, which is estimated as 20-30 times higher than conventional VPSA processes recently reported in the literature.

Acknowledgements

We would like to express our gratitude for the financial support from EPSRC (Grants No.: EP/F034520/1, EP/G062129/1, and EP/J018198/1) and KETEP (Grant No.: 2011-8510020030).

Nomenclature

A_c Column surface area (m^2)

b_i Equilibrium constant of component i (bar^{-1})

$b_{0,i}$ Pre-exponential equilibrium constant of component i (bar^{-1})

c_T Total concentration of the gas mixture (mol/m^3)

c_i Concentration of component i (mol/m^3)

$\hat{C}_{pg}$ Specific heat at constant pressure of the gas mixture (J/kg·K)

$\hat{C}_{vg}$ Specific heat at constant volume of the gas mixture (J/kg·K)

$\hat{C}_{ps}$ Specific heat of the solid (J/kg·K)

D_c Column diameter (m)

D_m Diffusivity of the gas mixture (m^2/s)

d_P Particle diameter (m)

D_z Axial mass dispersion coefficient (m^2/s)

F Molar flowrate (mol/s)

$(-\Delta H_i)$ Heat of adsorption of component i (J/mol)

h_w Heat transfer coefficient between the gas phase and the column wall ($W/m^2 \cdot K$)

k_g Thermal conductivity of the gas mixture (W/m·K)

$k_{LDF,i}$ LDF coefficient of component i (s^{-1})

k_z Axial thermal dispersion coefficient (W/m·K)

L_c Column length (m)

$\overline{M}$ Averaged molecular weight (kg/mol)

M_{ads} Mass of adsorbent (kg)

P Total pressure (bar)

P_i Partial pressure of component i (bar)

P_{ads} Adsorption pressure (bar)

P_{des} Desorption pressure (bar)

P_{feed} Feed pressure (bar)

Pr Prandtl number (-)

$\overline{q}_i$ Pellet averaged adsorbed phase concentration of component i (mol/m^3)

q^*_i Adsorbed phase concentration in the equilibrium state of component i (mol/m^3)

$q_{s,i}$ Saturation adsorption capacity of component i (mol/kg)

Q_{unit} Unit feed flowrate (m^3/s)

R Ideal gas constant (J/mol·K)

Re Reynolds number (-)

Sc Schimdt number (-)

t Time (s)

t_{cycle} Cycle time (s)

T Temperature (K)

T_{feed} Feed temperature (K)

T_w Wall temperature (K)

u Interstitial velocity (m/s)

y_i Molar fraction of component i (-)

z Spatial dimension (m)

Greek letters

α Valve opening rate (s^{-1})

γ Ratio of specific heats, C_p/C_v (-)

ε External bed void fraction (-)

μ Viscosity of gas mixture (Pa·s)

ρ_{ads} Adsorbed phase density (kg/m^3)

ρ_g Gas density (kg/m^3)

ρ_s Adsorbent density (kg/m^3)

References

Ahn H., Luberti M., Oreggioni G.D., 2014. A post-combustion CO_2 capture raid pressure/vacuum swing adsorption process and its application for decarbonizing a coal-fired power plant. 2014 AIChE Annual Meeting, Atlanta.

Ahn H., Luberti M., Liu Z., Brandani S., 2013. Process configuration studies of the amine capture process for coal-fired power plants. International Journal of Greenhouse Gas Control 16, 29–40.

Bird R. B., Stewart W. E., Lightfoot E. N., 2007. Transport Phenomena. 2nd ed. Wiley International.

Cho S. H., Park J. H., Beum H. T., Han S. S., Kim J. N., 2004. A 2-stage PSA process for the recovery of CO_2 from flue gas and its power consumption. Stud. Surf. Sci. Catal. 153, 405-410.

Delgado J. A., Uguina M. A., Sotelo J. L., Agueda V. I., Sanz A., Gomez P., 2011. Numerical analysis of CO_2 concentration and recovery from flue gas by a novel vacuum swing adsorption cycle. Computers & Chemical Engineering 35, 1010-1019.

Ergun S., 1952. Fluid flow through packed columns. Chem. Eng. Prog. 48, 89-94.

Figueroa J. D., Fout T., Plasynski S., McIlvried H., Srivastava R. D., 2008. Advances in CO_2 capture technology – The U.S. Department of Energy's Carbon Sequestration Program. International Journal of Greenhouse Gas Control 2, 9–20.

IPCC, 2005. Special report on carbon dioxide capture and storage.

IPCC, 2014. Fifth Assessment Report.

Kikkinides E. S., Yang R. T., 1993. Concentration and recovery of CO_2 from flue gas by Pressure Swing Adsorption. Ind. Chem. Eng. Res. 32, 2714-2720.

Ko D., Siriwardane R., Biegler L. T., 2003. Optimization of a pressure-swing adsorption process using zeolite 13X for CO_2 sequestration. Ind. Eng. Chem. Res. 42, 339-348.

Krishnamurthy S., Rao V. R., Guntuka S., Sharratt P., Haghpanah R., Rajendran A., Amanullah M., Karimi I. A., Farooq S., 2014. CO_2 capture from dry flue gas by vacuum swing adsorption: A pilot plant study. AIChE J. 60, 1830–1842.

Liu Z., Grande C. A., Li P., Yu J., Rodrigues A. E., 2011. Multi-bed vacuum pressure swing adsorption for carbon dioxide capture from flue gas. Sep. Purif. Tecnol. 81, 307-317.

Luberti M., Friedrich D., Brandani S., Ahn H., 2014. Design of a H_2 PSA for cogeneration of ultrapure hydrogen and power at an advanced integrated gasification combined cycle with pre-combustion capture. Adsorption 20, 511-524.

Luberti M., Kim Y.-H., Lee C.-H., Ferrari M.-C., Ahn H., 2015. New momentum and energy balance equations considering kinetic energy effect for mathematical modelling of a fixed bed adsorption column. Adsorption 21, 353–363.

Mollersten K., Yan J., Moreira J. R., 2003. Potential market niches for biomass energy with CO_2 capture and storage — opportunities for energy supply with negative CO_2 emissions. Biomass Bioenergy 25, 273–285.

Mukherjee S., Kumar P., Yang A., Fennell P., 2015. Energy and exergy analysis of chemical looping combustion technology and comparison with pre-combustion and oxy-fuel combustion technologies for CO_2 capture. Journal of Environmental Chemical Engineering 3, 2104–2114.

Myers A. L., 2002. Thermodynamics of adsorption in porous materials. AIChE J. 48, 145-160.

Obersteiner M., Azar C., Kauppi P., Mollersten K., Moreira J. R., Nilsson S., Read P., Riahi K., Schlamadinger B., Yamagata Y., Yan J., van Ypersele J.-P., 2001. Managing climate risk. Science 294, 786–787.

Oreggioni G. D., Brandani S., Luberti M., Baykan Y., Friedrich D., Ahn H., 2015. CO_2 capture from syngas by an adsorption process from a biomass gasification CHP plant: its comparison with amine-based CO_2 capture. International Journal of Greenhouse Gas Control 35, 71-81.

OriginLab, 2010. Data analysis and graphing software, Origin 8.5.

Park J. H., Beum H. T., Kim J. N., Cho S. H., 2002. Numerical analysis on the power consumption of the PSA process for recovering CO_2 from flue gas. Ind. Eng. Chem. Res. 41, 4122-4131.

Process System Enterprise Ltd, 2010. Available at http://www.psenterprise.com.

Rhodes J. S., Keith D. W., 2008. Biomass with capture: negative emissions within social and environmental constraints. Climate Change 87, 321-328.

Ruthven D. M., 1984. Principles of adsorption and adsorption processes, John Wiley & Sons.

Shen C., Liu Z., Li P., Yu J., 2012. Two-stage VPSA process for CO_2 capture from flue gas using activated carbon beads. Ind. Chem. Eng. Res. 51, 5011–5021.

Simader G. R., 2004. Case study: $2MW_{el}$ biomass gasification plant in Gussing (Austria). European Commission (Directorate-General for Energy and Transport).

Wakao N., Funazkri T., 1978. Effect of fluid dispersion coefficients on particle-to-fluid mass transfer coefficients in packed beds. Chemical Engineering Science 33, 1375-1384.

Wang L., Liu Z., Li P., Wang J., Yu J., 2012. CO_2 capture from flue gas by two successive VPSA units using 13XAPG. Adsorption 18, 445-459.

Wang L., Yang Y., Shen W., Kong X., Li P., Yu J., Rodrigues A. E., 2013. CO_2 capture from flue gas in an existing coal-fired power plant by two successive pilot-scale VPSA Units. Ind. Chem. Eng. Res. 52, 7947–7955.

Webley P. A., 2014. Adsorption technology for CO_2 separation and capture: a perspective. Adsorption 20, 225-231.

Xiao P., Zhang J., Webley P., Li G., Singh R., Todd R., 2008. Capture of CO_2 from flue gas streams with zeolite 13X by vacuum-pressure swing adsorption. Adsorption 14, 575–582.